IOP Publishing Nanotechnology
Nanotechnology **25** (2014) 455203 (7pp) doi:10.1088/0957-4484/25/45/455203

Incident-angle dependent color tuning from a single plasmonic chip

Guangyuan Si[1,4], Yanhui Zhao[2,4], Eunice Sok Ping Leong[3], Jiangtao Lv[1] and Yan Jun Liu[3]

[1] College of Information Science and Engineering, Northeastern University, Shenyang 110004, People's Republic of China
[2] Department of Engineering Science and Mechanics, The Pennsylvania State University, University Park, PA 16802, USA
[3] Institute of Materials Research and Engineering, Agency for Science, Technology and Research (A*STAR), 3 Research Link, 117602, Singapore

E-mail: liuy@imre.a-star.edu.sg

Received 30 July 2014, revised 12 September 2014
Accepted for publication 22 September 2014
Published 22 October 2014

Abstract

We report on a broad color tuning effect covering the visible range from a single plasmonic chip. By simply tilting the orientation of the designed plasmonic chip within a certain range, the photon–plasmon coupling interactions between the incident light and the plasmonic nanostructures on the chip can be finely tuned, resulting in an angle-dependent continuous color filtering effect. The physical mechanism of the device is investigated through the full-wave calculations, which provide important guidance for the design and optimization of the proposed devices. The broad color tuning from the demonstrated single chip will potentially benefit visualization and display technologies, and is particularly useful for the construction of reflection-based spatial light modulators.

Keywords: color filter, nanorod, plasmon resonance

(Some figures may appear in colour only in the online journal)

1. Introduction

The display techniques thus far have reached a stage that requires high-resolution pixel sizes, high efficiency, and low power consumption for the increasing demand on splendid visual effects from handhold devices to large screen light-emitting diode televisions. Among all the factors that affect the visual effect, the color pixel seems to be the most fundamental unit that affects displaying quality significantly in terms of image resolution, contrast, color themes and saturation. Generally, the vivid colors from almost all liquid crystal displays are created from the composition of three different colors (red, green, and blue, also known as primary colors [1, 2]) that are filtered by the color filters placed between the panel screen and the backlight sources. The footprint of a color filter is a critical parameter that affects the performance of a whole display. Traditional color filters employing organic dyes or chemical pigments usually suffer from performance degradation when they are exposed to long-duration (or strong intensity) ultraviolet irradiation or high temperature environment. Inspired by natural color filtering (the wings of Morpho butterflies, for instance), structural color is an attractive and ideal candidate for colorant pigmentation employed by the current display technologies. Various photonic crystal and plasmonic nanostructures have been developed to demonstrate the structural color filtering function [3–20]. Particularly, single-layer metallic nanostructures have irreplaceable advantages over materials based on colorant pigmentation since they are robust, antifading, and integratable. In an effort to further reduce the dimensions of color pixels, plasmon-based color filters can significantly shrink the size of single color pixels down to the micron or even sub-micron level [21, 22], allowing for the deployment of more pixel numbers within the same confined area and thereby leading to significantly improved display resolutions

[4] These authors contributed equally to this work.

 © 2014 IOP Publishing Ltd Printed in the UK

and color saturations in accordance with the development of driving circuits.

So far, color filters working under transmission mode have been extensively studied [23–34]. Such devices require the transmission of light at certain frequencies with all the other ranges either blocked or reflected back to the incident plane. Classical designs have been demonstrated using nanoslits [30], nanohole arrays [35, 36] or metal–dielectric–metal (MDM) stacks [37]. For one-dimensional (1D) nanoslits or MDM stacks, the intrinsic properties of 1D gratings downgrade their performance when dealing with transverse electric polarized light. For nanoholes, the transmission peaks can be tuned by changing the periodicity of the array; however, the intensity varies abruptly with increasing hole sizes, making nanoholes a less promising candidate for constructing plasmonic color filters. In addition, low transmission efficiency of hole-array plasmonic color filters also limits their commercial applications. Therefore, it is highly desirable to design elegant plasmonic color filters with both high efficiency and simple architectures, especially for reflection-mode ones (like the e-ink technology currently used in Kindle e-readers). Here, we demonstrate color filters operating under reflection mode with incident-angle dependency. The color filters consist of a nanorod array fabricated by laser interference lithography (LIL) and ion milling (IM) techniques. In a previous work, we have shown the feasibility of passive filtering out individual colors under reflection mode using nanorod arrays with ultrasmall inter-rod spacing and varying array periodicities [11]. In this work, we investigate a new mechanism on continuous color tuning through tilting a single chip. In our efforts to achieve such a powerful plasmonic chip, the underlying mechanism of the color generation is investigated, which is attributed to the photon–plasmon coupling between the incident light and the nanorod array. The immediate application of such a plasmonic color chip would be integrated with a reflection-based digital micromirror device (DMD) to realize visual effects or color displays. Its huge potential on many other optical applications related to display techniques can also be expected and readily actualized.

2. Design and experiment

2.1. Design principle

Our design concept is to utilize the photon–plasmon coupling effect between the nanorod structures and the illuminating light at different incident angles to achieve tunable resonances in visible frequencies. The coupling between plasmonic nanostructures and external electromagnetic waves is a complicated process that involves many interactions at the same time [38, 39]. Figure 1(a) is the schematic showing the working mechanism of the proposed plasmonic chip for visible color tuning. In this case, the nanorod array is employed as the basic structure for filtering out individual colors, under the consideration that proper volumetric ratio between nanorods and free space will ensure a proper degree of coupling between the incident light and the nanorod array.

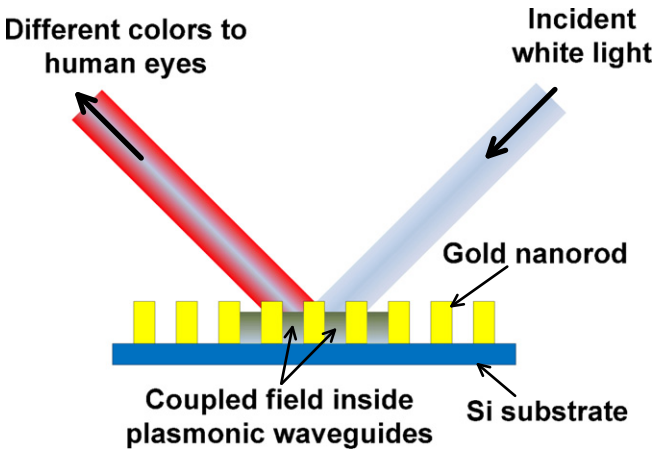

Figure 1. Sketch showing the working mechanism of the proposed plasmonic chip for continuous color tuning.

It has been revealed from our previous experiences on constructing reflective plasmonic color filters [11] that the coupling effects play key roles in generating wavelength-selective colors when the gap distance between adjacent nanorods is less than 50 nm. The plasmon coupling will become weak as the gap increases. At a certain gap distance, only localized surface plasmon resonance (LSPR) will dominate, which applies to our design discussed here. LSPR can be estimated using the coupling dipole theory, which has been developed and discussed comprehensively elsewhere [38–41]. Each single nanorod can be modeled by a dipole of polarizability α, which can be written as [42]:

$$\alpha^{\text{static}} \propto V\frac{\varepsilon_{\text{m}} - \varepsilon_{\text{d}}}{3\varepsilon_{\text{m}} + 3\chi(\varepsilon_{\text{m}} - \varepsilon_{\text{d}})}, \tag{1}$$

where ε_{m} and ε_{d} are the relative permittivity of metal and the surrounding dielectric, respectively, χ is the shape factor relating to the physical shape of the nanorod and V is the volume of the nanorod. When the nanorod array is excited by an electromagnetic field with frequency ω, the rod dipole will radiate a scattering field in proportion to its dipole moment. The total LSPR field with an effective polarizability α^* is a combined effect of the incident field and radiations from each individual nanorods, which can be expressed as [42]:

$$\alpha^* = \frac{1}{1/\alpha - S}, \tag{2}$$

with the array factor S being the retarded dipole sum, indicating the collective contributions from all the other dipole impacting on the interested particles [43, 44] and depending on the geometric factors of the nanorods. The S factor for a square array of nanorods under normal incidence can be written as [42]:

$$S = \sum_{\text{dipoles}} \mathrm{e}^{\mathrm{i}kr}\left[\frac{(1 - \mathrm{i}kr)\left(3\cos^2\theta - 1\right)}{r^3} + \frac{k^2\sin^2\theta}{r}\right], \tag{3}$$

where θ is the angle between the position vector and the

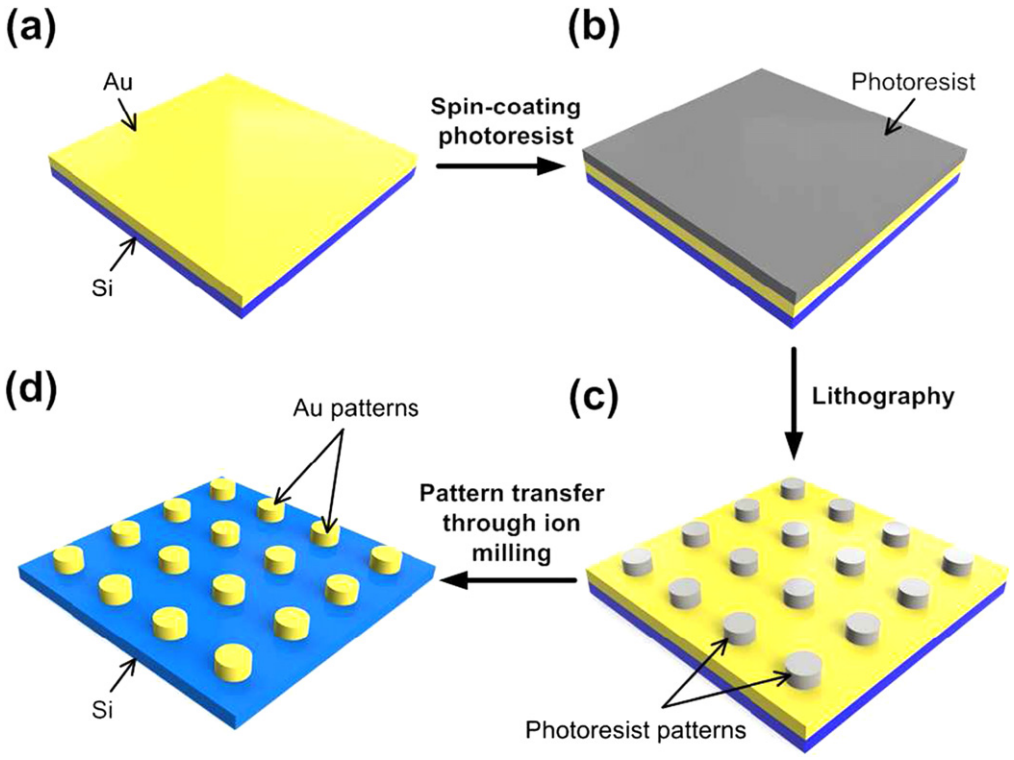

Figure 2. Schematic showing the process flow of the sample fabrication. (a) Au film deposition on a Si substrate. (b) Spin-coating of the photoresist on the Au film. (c) Two dimensional photoresist patterning by LIL. (d) Au nanorod arrays by pattern transfer via argon IM.

polarization direction. Depending on the geometries of the nanostructures, S may contribute to radiative damping or dynamic depolarization effects, and can be solved numerically. From equation (2), a peak in the reflection spectrum can be achieved when the condition $S = 1/\alpha$ is satisfied, which involves the impacts of different incident angles on the resonance frequencies. This reflection peak corresponds to a certain color, which can be therefore used to design reflective color filters.

2.2. Fabrication

The fabrication of large-area gold (Au) nanorod array residing on a silicon (Si) substrate follows standard procedure for nanofabrication. The detailed process steps of fabrication are illustrated in figure 2. The key steps of fabrication involve electron-beam (e-beam) evaporation, LIL and IM. Si substrates were first cleaned using a standard ultrasonic bath with acetone, isopropanol alcohol and deionized water, respectively, and finally blew dry with a nitrogen gun. Then the samples were put into the vacuum chamber of an e-beam evaporator (Edwards Auto 306) for metal film deposition. 8 nm titanium (not shown in figure 2) and 200 nm Au were sequentially deposited at an average evaporation rate of 0.04 nm s^{-1} under the vacuum condition of $\sim 4 \times 10^{-7}$ mbar. Spin-coating of positive photoresist (S1805, Dow, Midland, MI, USA) onto the Au surface was conducted at 2000 rpm for 30 s, followed by a baking process at 90 °C for 15 min.

To pattern the photoresist, the sample was exposed twice under Lloyd's LIL setup by rotating 90°. The laser wavelength was 325 nm. The periodical distance of the photoresist pattern was controlled to be 450 nm by adjusting the incident angle. After development, the sample was ion-milled to transfer patterns from photoresist to the Au film using an ion beam etcher (argon source, INTLVAC NANOQUEST). During the milling process, all samples were fixed to a working plate which was cooled and rotated at a constant speed to ensure even uniformity of the ion bombardment. The argon ions impinged on the sample surface at a slightly titled degree to the normal of the sample surface, and this is to ensure a uniform milling rate and homogeneous profiles over the whole sample surface. The beam voltage was set to 300 V with 45 V accelerating voltage, 110 mA beam current, and 8 mA accelerating current. The total milling time was around 10 min with the power stabilized at ~160 W.

2.3. Simulation

Our color filter nanochip was calculated using CST Microwave Studio. In the simulation domain, one unit cell was considered which consisted of a vertically oriented cylindrical Au nanorod residing on a Si substrate half space. The nanorod had a radius of $r = 100$ nm and a height of $h = 200$ nm. Periodic boundary conditions were assigned to the lateral walls and floquet ports were imposed on the top and bottom of the unit cell to mimic an infinite periodic array with the periodicity of $p = 450$ nm. A fifth order Drude–Lorentz model was employed to fit the measured permittivity of Au [45] while the permittivity of Si was quoted elsewhere [46].

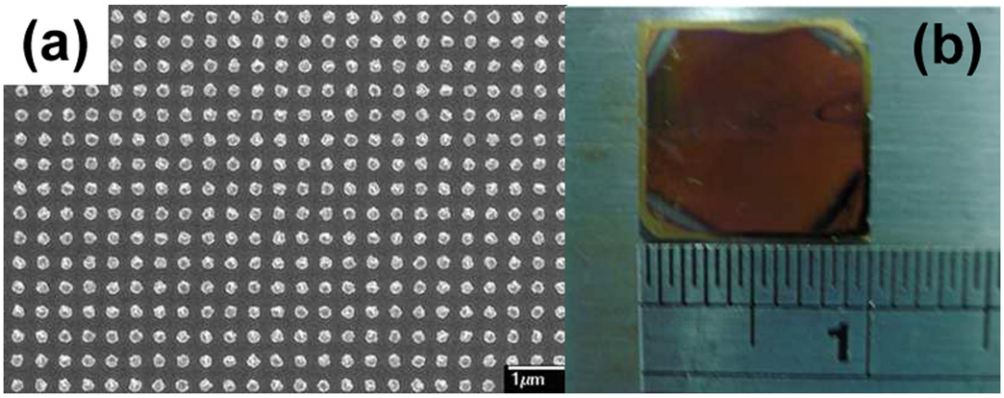

Figure 3. (a) Typical SEM image of the nanorod array fabricated by LIL and IM. (b) The optical image of a real sample with 1 cm × 1 cm size.

3. Results and discussion

The overview scanning electron microscopy (SEM) image of our plasmonic nanorod chip is shown in figure 3(a). Figure 3(b) is the optical image of the chip with a large dimension. Our fabrication method based on LIL and IM is capable of creating such nanorod arrays with working areas from sub-micrometer to centimeter scale. The demonstrated sample is two dimensional patterns with its size around 1 cm × 1 cm.

Figure 4(a) shows the reflection curves at different incident angles, which are normalized to the maximum reflectivity at each respective incident angle. It can be seen that the reflection peak redshifts with increasing incident angle from 30° to 70°. The reflection band moves from 420–490 nm to 630–680 nm, indicating that the color of the nanostructure appears blue at small incident angle and gradually changes to red as the incident angle increases. The magnetic field distributions near the interface between the nanorod array and the Si substrate are presented in figure 4(b) at various wavelengths for incident angles of 30°, 50°, and 70°, respectively. It is observed that at the reflection peak position for each incident angle, the magnetic field exhibits a curl-like pattern, concentrating near the vertical surface of the nanorods. In the other cases, no antiparallel magnetic fields exist on opposite sides of the nanorod vertical walls. The fields become strong in the air-gap region between adjacent nanorods. This behavior of magnetic fields indicates the existence of localized magnetic surface plasmon polariton (LMSPP) mode [47, 48] due to the current induced along the vertical walls of the Au nanorods by the longitudinal electric field component of the incident wave. As the angle of incidence increases, stronger longitudinal electric field provided by the incident wave excites the LMSPP mode at a longer wavelength, leading to the observed 'color-tuning' effect of the plasmonic chip.

One should also note that under the illumination of a plane wave at an incident angle of θ_i, the nanostructure is capable of supporting one or more higher order floquet modes (i.e., diffraction modes) due to the large periodicity with the transverse wave number of $k_t = k_0 \sin\theta_i + 2\pi n/p$, where n is an integer. For a specific n, its corresponding floquet mode

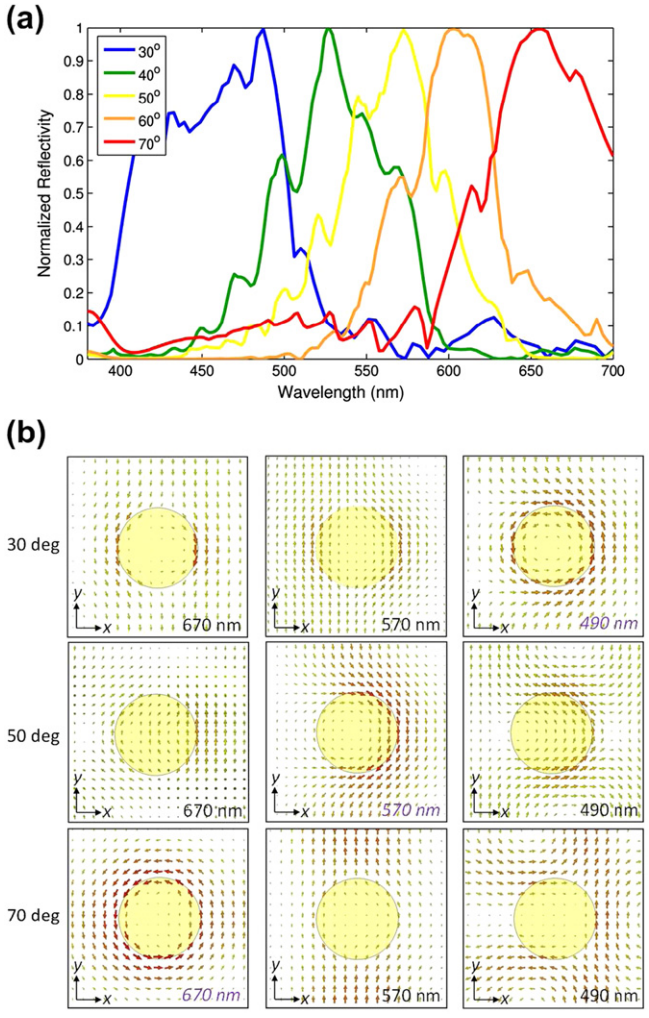

Figure 4. (a) Normalized specular reflections for various angles of incidence. (b) Magnetic field distributions near the interface between the nanorod array and the Si substrate at varying incident angles of 30 (top row), 50 (middle row), and 70 (bottom row) degrees and different wavelengths of 670 (left column), 570 (middle column), and 490 (right column) nm.

belongs to a propagating mode if $k_t \leqslant k_0$ is satisfied. In our case, the higher order diffraction modes are propagating modes only when n is a negative integer. This means that the reflected wave caused by diffraction lies on the same side of

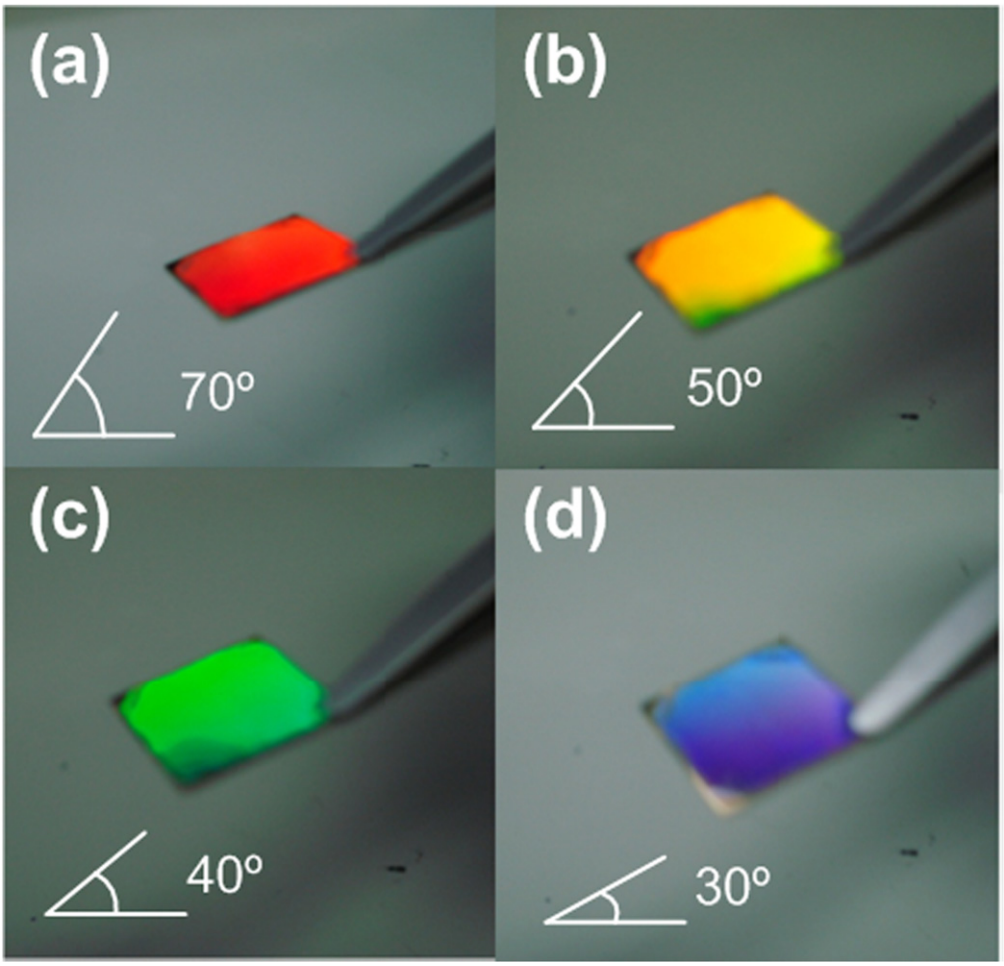

Figure 5. Optical images of the same sample of Au nanorods on a Si substrate taken from varying incident angles. Different vivid colors of (a) red, (b) yellow, (c) green, and (d) blue are shown. Redshift of resonance colors with increasing tilting angles can be clearly observed.

the nanostructure–air interface normal with that of the incident wave and therefore will not be collected by the detector. Since there is no cavities presented in such structures and size/height ratios in most cases are large enough to be considered as a metasurface, nanorods or nanodiscs allow strong interaction between the sample surface and the incident light, leading to color filtering effect achieved by trapping the undesired frequencies in the form of either propagation modes or coupling/de-coupling processes. In addition, the color filtering effect could be also designed by exploiting the constructive interference between the light directly reflected by the Si substrate and the scattered light by Au nanorods, which may provide a sharper resonance peak but limited tuning range.

The proof-of-concept results captured by a handheld camera (Sony DSC-W70) are shown in figure 5. The volume ratio of each unit cell allows effective interaction of the nanorod with the broadband incident light source. By simply tilting the same sample to different observation angles under the same illumination conditions, individual colors can be filtered out. Note that the observation angle was manually measured using a protractor with the accuracy of ±3°. It can be clearly observed that primary colors including red, yellow, green, and blue can be generated by reducing the tilting angles starting from the normal incidence. The unclear colorant displayed near the four corners of the sample surface is caused by fabrication imperfections (i.e., non-uniform distribution of photoresist during spin coating) caused by sample handling during the preparation process. The large size of color filter shown here is for the purpose of demonstration only, it can be easily shrink down to micrometer scale while maintaining similar functionality; however, due to the collective resonance effects on the filtering from a large number of nanorod units, we expect that the intensity of generated colors from a small number of nanorods will decrease. It is also worth mentioning that continuous tuning of plasmon resonance can be also achieved by actively varying the refractive index of the surrounding medium. Liquid crystal is a well-know active medium that has been widely used to tune the optical properties of plasmonic devices [49–56]. However, subject to the limited change of the refractive index, these liquid-crystal-based plasmonic devices only give a narrow tuning range (less than 100 nm in wavelength). In contrast, the plasmonic chip demonstrated in this work has a much broader color tuning range (the whole visible range) by simply tilting, making it more promising for applications based on color-visualization.

Based on our previous experiences, color filters working under reflection mode have better efficiency or intensity as compared with color filters working under transmission mode. The reflective color filters with a working area of 10–20 μm^2 would provide very good visibility for practical usage. Conventional DMD for spatial light modulation works in the way that a micromirror in an array is controlled to alter its orientation to modulate the light path reflected by the micromirror. It is often used in a digital light processing (DLP) device such as a projector for displays. DMD itself can only provide grayscale images due to its working mechanism, and it has to be combined with other techniques to achieve the color display in a projector. The color display based on DMD can only be generated by either inserting a color wheel between the light source and DMD, or introducing three light sources (primary colors). Our work on the angle-dependent color filters will fill in this gap allowing the phase tuning and color selection at the same time. It has huge potentials in DLP devices, especially for DMD based displaying techniques. In addition, the pixel size can be further reduced to improve the resolution of the DMD, leading to a better imaging resolution for display, or high accuracy for optical manipulation techniques such as optical tweezers.

4. Conclusion

In summary, we have demonstrated a large-area plasmonic nanorod array fabricated by combining LIL and IM techniques. Incident-angle-dependent continuous color tuning has been achieved using the single chip with fixed structural parameters. The underlying physical mechanism was the modification of the photon–plasmon coupling between the incident light and the plasmonic nanostructures via tilting the orientation of the plasmonic chip, which was confirmed by the full-wave calculations. The plasmonic chip works in reflection mode, making it promising to integrate with DMDs for light modulation and display applications.

Acknowledgments

This work was supported by Natural Science Foundation of Hebei Province (Grant No. A2013501049 and F2014501127), Science and Technology Research Funds for Higher Education of Hebei Province (Grant No. ZD20132011), Fundamental Research Funds for the Central Universities (Grant No. N120323002), and Science and Technology Foundation of Liaoning Province (Grant No. 20131031). We thank Z H Jiang and B Q Lu for fruitful discussions.

References

[1] He G, Guo D, He C, Zhang X, Zhao X and Duan C 2009 *Angew. Chem., Int. Ed. Engl.* **48** 6132
[2] Seo J H, Seo J H, Park J H, Kim Y K, Kim J H, Hyung G W, Lee K H and Yoon S S 2007 *Appl. Phys. Lett.* **90** 203507
[3] Lee S K, Yi G R, Moon J H, Yang S M and Pine D J 2006 *Adv. Mater.* **18** 2111
[4] Cho E H, Kim H S, Cheong B H, Oleg P, Xianyua W, Sohn J S, Ma D J, Choi H Y, Park N C and Park Y P 2009 *Opt. Express* **17** 8621
[5] Arsenault A C, Puzzo D P, Manners I and Ozin G A 2007 *Nat. Photonics* **1** 468
[6] Koyama S, Inaba Y, Kasano M and Murata T 2008 *IEEE Trans. Electron Device* **55** 754
[7] Inaba Y, Kasano M, Tanaka K and Yamaguchi T 2006 *IEEE Electron Device Lett.* **27** 457
[8] Cho E H, Kim H S, Sohn J S, Moon C Y, Park M C and Park Y P 2010 *Opt. Express* **18** 27712
[9] Chen Q, Chitnis D, Walls K, Drysdale T D, Collins S and Cumming D R S 2012 *IEEE Photonics Technol. Lett.* **24** 197
[10] Chen Q and Cumming D R S 2010 *Opt. Express* **18** 14056
[11] Si G *et al* 2013 *Nanoscale* **5** 6243
[12] Xu T, Wu Y K, Luo X and Guo L J 2010 *Nat. Commun.* **1** 59
[13] Wu Y K R, Hollowell A E, Zhang C and Guo L J 2013 *Sci. Rep.* **3** 1194
[14] Ellenbogen T, Seo K and Crozier K B 2012 *Nano Lett.* **12** 1026
[15] Burgos S P, Yokogawa S and Atwater H A 2013 *ACS Nano* **7** 10038
[16] Diest K, Dionne J A, Spain M and Atwater H A 2009 *Nano Lett.* **9** 2579
[17] Zhao Y, Xie Z, Gu H, Zhu C and Gu Z 2012 *Chem. Soc. Rev.* **41** 3297
[18] Cai Z, Liu Y J, Teng J and Lu X 2012 *ACS Appl. Mater. Interfaces* **4** 5562
[19] Knop K 1978 *Appl. Opt.* **17** 3598
[20] De Sio L, Caligiuri V and Umeton C 2014 *J. Opt.* **16** 065703
[21] Kumar K, Duan H, Hegde R S, Koh S C W, Wei J N and Yang J K W 2012 *Nat. Nanotechnology* **7** 557
[22] Tan S J, Zhang L, Zhu D, Goh X M, Wang Y M, Kumar K, Qiu C W and Yang J K W 2014 *Nano Lett.* **14** 4023
[23] Zeng B, Gao Y and Bartoli F J 2013 *Sci. Rep.* **3** 2840
[24] Do Y S, Park J H, Hwang B Y, Lee S M, Ju B K and Choi K C 2013 *Adv. Opt. Mater.* **1** 133
[25] Yokogawa S, Burgos S P and Atwater H A 2012 *Nano Lett.* **12** 4349
[26] Park C H, Yoon Y T, Shrestha V R, Park C S, Lee S S and Kim E S 2013 *Opt. Express* **21** 28783
[27] McCrindle I J H, Grant J, Drysdale T D and Cumming D R S 2014 *Adv. Opt. Mater.* **2** 149
[28] Si G, Zhao Y, Liu H, Teo S, Zhang M, Huang T J, Danner A J and Teng J 2011 *Appl. Phys. Lett.* **99** 033105
[29] Liu Y J, Si G Y, Leong E S P, Xiang N, Danner A J and Teng J H 2012 *Adv. Mater.* **24** OP131
[30] Laux E, Genet C, Skauli T and Ebbesen T W 2008 *Nat. Photonics* **2** 161
[31] Liu Y J, Si G Y, Leong E S P, Wang B, Danner A J, Yuan X C and Teng J H 2012 *Appl. Phys.* A **107** 49
[32] Lee H S, Yoon Y T, Lee S S, Kim S H and Lee K D 2007 *Opt. Express* **15** 15457
[33] Inoue D, Miura A, Nomura T, Fujikawa H, Sato K, Ikeda N, Tsuya D, Sugimoto Y and Koide Y 2011 *Appl. Phys. Lett.* **98** 093113
[34] Yu C J, Liang Y P, Hong H F and Wang C M 2012 *Opt. Eng.* **51** 044001
[35] Barnes W L, Dereux A and Ebbesen T W 2003 *Nature* **424** 824
[36] Genet C and Ebbesen T W 2007 *Nature* **445** 39
[37] Cai W, Chettiar U K, Yuan H K, de Silva V C, Kildishev A V, Drachev V P and Shalaev V M 2007 *Opt. Express* **15** 3333
[38] Lee K and Wei P 2010 *Small* **6** 1900
[39] Leong E S P, Wu S J, Zhang N, Loh W W, Khoo E H, Si G Y, Dai H T and Liu Y J 2014 *Nanotechnology* **25** 055203
[40] Markel V A and Sarychev A K 2007 *Phys. Rev. B: Condens. Matter Mater. Phys.* **75** 085426
[41] Zou S and Schatz G C 2006 *Nanotechnology* **17** 2813

[42] Auguie B and Barnes W L 2008 *Phys. Rev. Lett.* **101** 143902
[43] Zou S, Janel N and Schatz G C 2004 *J. Chem. Phys.* **120** 10871
[44] Markel V A 2005 *J. Phys. B: At. Mol. Opt. Phys.* **38** L115
[45] Johnson P B and Christy R W 1972 *Phys. Rev.* B **6** 4370
[46] Bass M *et al* 2009 *Handbook of Optics* (New York: McGraw-Hill)
[47] Jiang Z H, Yun S, Toor F, Werner D H and Mayer T S 2011 *ACS Nano* **5** 4641
[48] Yun S, Jiang Z H, Xu Q, Liu Z, Werner D H and Mayer T S 2012 *ACS Nano* **6** 4475
[49] Kossyrev P A, Yin A, Cloutier S G, Cardimona D A, Huang D, Alsing P M and Xu J M 2005 *Nano Lett.* **5** 1978
[50] Hsiao V K S, Zheng Y B, Juluri B K and Huang T J 2008 *Adv. Mater.* **20** 3528
[51] Liu Y J, Hao Q Z, Smalley J S T, Liou J, Khoo I C and Huang T J 2010 *Appl. Phys. Lett.* **97** 091101
[52] Liu Y J, Zheng Y B, Liou J, Chiang I-K, Khoo I C and Huang T J 2011 *J. Phys. Chem.* C **115** 7717
[53] Liu Y J, Leong E S P, Wang B and Teng J H 2011 *Plasmonics* **6** 659
[54] De Sio L, Klein G, Serak S, Tabiryan N, Cunningham A, Tone C M, Ciuchi F, Bürgi T, Umeton C and Bunning T 2013 *J. Mater. Chem.* C **1** 7483
[55] De Sio L, Placido T, Serak S, Comparelli R, Tamborra M, Tabiryan N, Curri M L, Bartolino R, Umeton C and Bunning T 2013 *Adv. Opt. Mater.* **1** 899
[56] Si G Y, Zhao Y H, Leong E S P and Liu Y J 2014 *Materials* **7** 1296